

Strength and stability analysis of a single-walled black phosphorus tube under axial compression

This content has been downloaded from IOPscience. Please scroll down to see the full text.

2016 Nanotechnology 27 275701

(<http://iopscience.iop.org/0957-4484/27/27/275701>)

View [the table of contents for this issue](#), or go to the [journal homepage](#) for more

Download details:

IP Address: 130.56.64.29

This content was downloaded on 23/05/2016 at 10:36

Please note that [terms and conditions apply](#).

Strength and stability analysis of a single-walled black phosphorus tube under axial compression

Kun Cai^{1,2}, Jing Wan¹, Ning Wei¹ and Qing H Qin²

¹College of Water Resources and Architectural Engineering, Northwest A&F University, Yangling 712100, People's Republic of China

²Research School of Engineering, the Australian National University, Canberra, ACT, 2601, Australia

E-mail: qinghua.qin@anu.edu.au

Received 8 April 2016, revised 21 April 2016

Accepted for publication 5 May 2016

Published 23 May 2016



CrossMark

Abstract

Few-layered black phosphorus materials currently attract much attention due to their special electronic properties. As a consequence, a single-layer black phosphorus (SLBP) nanotube has been theoretically built. The corresponding electronic properties of such a black phosphorus nanotube (BPNT) were also evaluated numerically. However, unlike graphene formed with $2sp^2$ covalent carbon atoms, SLBP is formed with $3sp^3$ bonded atoms. It means that the structure from SLBP will possess lower Young's modulus and mechanical strength than those of carbon nanotubes. In this study, molecular dynamics simulation is performed to investigate the strength and stability of BPNTs affected by the factors of diameter, length, loading speed and temperature. Results are fundamental for investigating the other physical properties of a BPNT acting as a component in a nanodevice. For example, buckling of the BPNT happens earlier than fracture, before which the nanostructure has very small axial strain. For the same BPNT, a higher load speed results in lower critical axial strain and a nanotube with lower axial strain can still be stable at a higher temperature.

 Online supplementary data available from stacks.iop.org/NANO/27/275701/mmedia

Keywords: black phosphorus, nanotube, molecular dynamics, fracture, buckling

(Some figures may appear in colour only in the online journal)

1. Introduction

In recent years, as a new two-dimensional semiconductor material, few-layer black phosphorus has been shown to have excellent electronic properties [1–4] as compared with graphene [5, 6] boron nitride [7, 8] and MoS_2 [9, 10]. Considering such excellent material properties, much effort has been put into researching its potential applications. Unlike graphene, which is formed with $2sp^2$ carbon atoms, single-layer black phosphorus (SLBP or phosphorene) is formed by bonding phosphorus atoms together with $3sp^3$ hybridized bonds. The interlayer interaction of many-layered black phosphorus is mainly due to the van der Waals attraction [11]. Hence, the in-plane strength and stiffness of SLBP is not as

high as those of the graphene [6]. Obviously, for a component containing SLBP in a nanodevice, the strength and stability of the structure are fundamental to ensure the normal operation of the device. The mechanical properties of a SLBP have been investigated thoroughly during the past decade. For example, on testing the in-plane moduli of SLBP along different directions, Jiang and Park [12] claimed that the elastic modulus is ~ 106.4 GPa along the pucker direction and ~ 41.3 GPa in its vertical direction. They also discovered [13] that the out-of-plane Poisson's ratio of SLBP is negative when SLBP is under uniaxial tension along the pucker direction. In contrast, the modulus reported by Wei and Peng [14] is ~ 44 GPa only. In the following work, the ideal tensile strength and critical strain of SLBP are discussed. Wang *et al* [15] obtained the

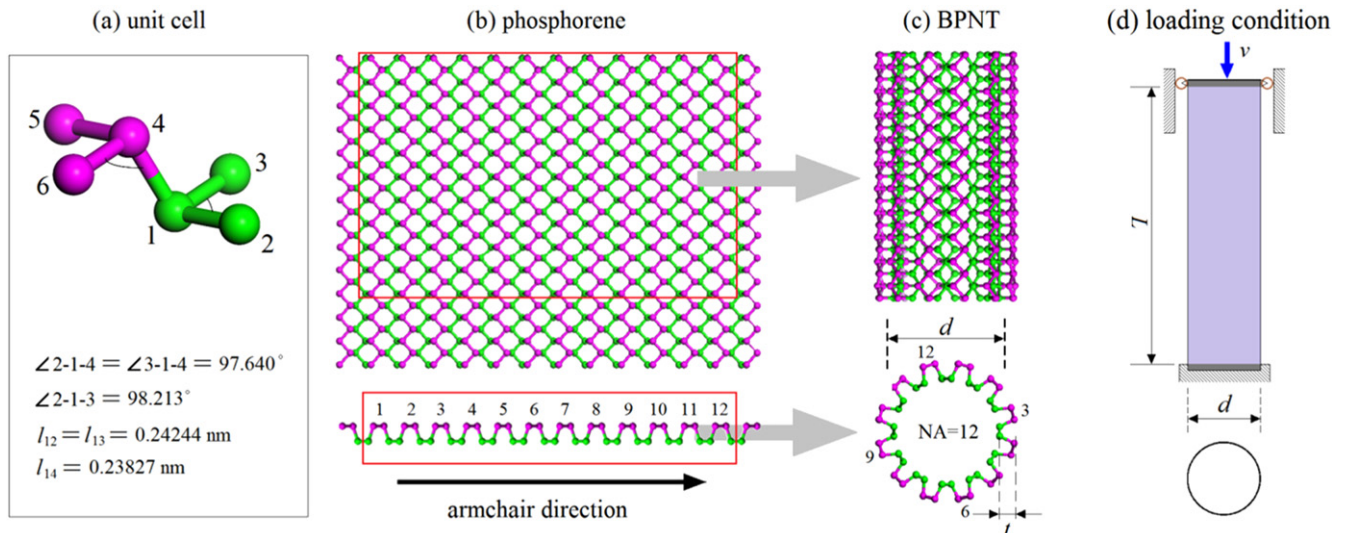


Figure 1. Geometrical model of a black phosphorus nanotube (BPNT). (a) The unit cell of single-layer black phosphorus (SLBP). (b) A nanoribbon of single-layer phosphorene. (c) The BPNT was obtained by curling the ribbon within the red frame in (b) along the armchair direction. In the model, $NA = 12$ means that there are 12 periodic unit cells along the circular direction (i.e., the curved armchair direction). ' d ' is the average diameter of the BPNT, i.e., half of the summation of the diameters of the two layers. ' t ' is the thickness of SLBP. (d) The loading condition for a BPNT under uniaxial compression. ' v ' is the velocity of the left end during loading. The gray areas of the tube are fixed on the degrees of freedom within the cross section of the tube. In this study, the thickness of each gray area is 0.1657 nm. ' L ' is the effective length of tube, which is 0.3314 nm shorter than the total length of tube (L^*).

same value of the modulus in their study on the dynamics behavior of a nanoresonator made of black phosphorus. Besides elastic modulus, researchers have also investigated such mechanical properties as the edge stress of SLBP [16], the coupling of mechanical deformation and electrical properties [17], SLBP under shear load [18] and the fracture limits of SLBP [19]. Hence, the mechanical properties are important for designing a nanodevice with black phosphorus sheets.

Similar to the formation of a carbon nanotube [20–24] by curling a piece of graphene ribbon along one direction, researchers also suggested that a nanotube could be made from a SLBP nanoribbon. Indeed, some properties of a black phosphorus nanotube (BPNT) have been estimated using numerical methods [25]. It is, however, still necessary to demonstrate the relationship between the material properties of a nanostructure and its strength and stability. In our previous work [26], we have found that a BPNT formed by curling SLBP along different directions (e.g., armchair/pucker direction and zigzag direction) has different stability behaviors at finite temperature. In a word, just the thermal vibration of atoms on a BPNT at high temperature may lead to the collapse of the nanostructure. In the present study, we focus on the strength and stability of a BPNT under axial compression. Some factors affecting the design of a future nanodevice with BPNT components, such as the slenderness, length, loading speed and temperature of the environment are investigated. From our previous study [26], the zigzag BPNT was found to have poorer stability than the armchair BPNT. Hence, only the armchair BPNT is considered in the present study.

Table 1. Parameters of BPNTs in discussion on the effect of diameter. $\alpha^* = L^*/d$, $L = L^* - 0.3314 \text{ nm}$, $\alpha = L/d$.

	Model 1	Model 2	Model 3	Model 4	Model 5
NA	14	16	18	20	22
d/nm	1.951	2.221	2.507	2.785	3.065
L^*/nm	15.576	17.896	20.050	22.204	24.524
α^*	7.9836	8.0576	7.9976	7.9727	8.0013
L/nm	15.245	17.565	19.719	21.873	24.193
α	7.8137	7.9084	7.8654	7.8537	7.8932

2. Models and method

Figure 1 demonstrates a BPNT made from SLBP by the geometrical mapping method. Figure 1(d) presents loading conditions of a cylindrical tube with average diameter of ' d ' for the mechanical model used in the present simulation. The atoms within the gray area are fixed during simulation. Four factors are considered in the following analysis. The first one is the effect of the diameter of tube. The parameters of tubes involved are listed in table 1. The second is the length effect. In discussing the length effect, tubes with the same diameter (or $NA = 20$, or $d = 2.785 \text{ nm}$) have different lengths. The third is the effect of loading speed (or value of v). In the discussion, the tube with $NA = 20$ and $L = 20.166 \text{ nm}$ is adopted. The final factor is the temperature effect. For the strength and stability of the BPNT with $NA = 20$ and $L = 20.166 \text{ nm}$, the environmental temperature increases from 0.1 K to the critical value at which the tube is either fractured or has global buckling. Details are given in the following sections.

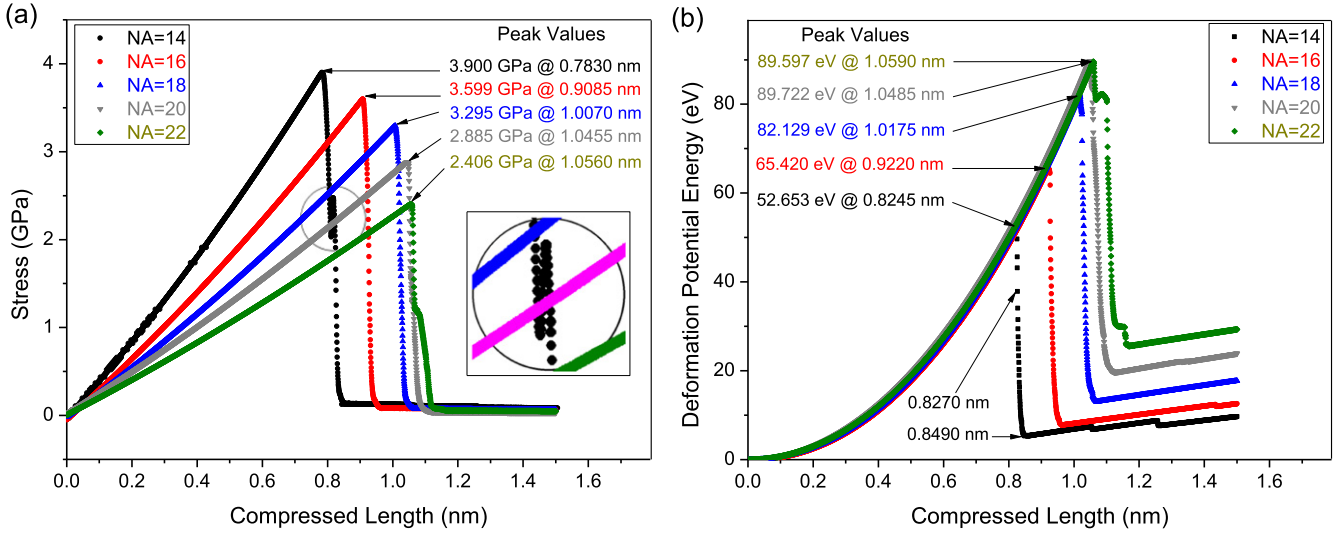


Figure 2. The stress and deformation potential energy of the BPNTs (with the same value of α) under compression. (a) The stress versus compressed length curve. The stress is the average value of the axial force over the cross-sectional area of tube. (b) The deformation potential energy (DPE) versus compressed length curve. The initial potential energy of the five cases is -1385.55 (NA = 14), -1831.95 (NA = 16), -2320.17 (NA = 18), -2864.74 (NA = 20) and -3489.21 eV (NA = 22), respectively.

The open code for molecular dynamics simulation [27] is used in the present study. Meanwhile, the Stillinger–Weber (S–W) potential developed by Jiang *et al* [28] is used to model the interaction among atoms in a BPNT.

The major steps in molecular dynamics simulation here are as follows. (1) Create a BPNT (e.g., with specified value of NA and L or L^*). (2) Reshape the tube by energy minimization using the steepest descent algorithm. (3) Take a thermal bath for the tube in the canonical NVT ensemble with $T = 0.1$ K for 50 ps. (4) Initiate the velocities of atoms to be zero and fixed the atoms (in the gray areas in figure 1(d)) at two ends of the tube. (5) Keep the free atoms in the above NVT ensemble and, simultaneously, start the displacement loading step. In each loading step, the upper end of the tube moves down by ‘ s ’ within 1 time step (i.e., 1 fs) but followed with ‘ t_R ’ period of relaxation. (6) Stop the loading step when buckling/fracture of the BPNT clearly occurs.

3. Results and discussion

3.1. Effect of nanotube diameter on the strength and stability of BPNTs

In this section, five BPNTs are involved in simulation to demonstrate the effect of diameter on the strength and stability of BPNT as they have similar ratios of length over diameter. The geometrical parameters of the tubes are listed in table 1, i.e., NA = 12, 14, 16, 18, 20, 22. The velocity of the load is set by specifying $s = 0.0005$ nm and it is followed with 2 ps of relaxation (i.e., $t_R = 2$ ps).

Due to the different initial lengths of BPNTs, only the accumulation of the displacement load acts as the level axis in the following curve figures.

From figure 2(a), one can find that the maximal value of stress decreases with the increase of the diameter of the tube

(or NA). This can be explained from Euler’s buckling formulation for buckling of a linear elastic column [29, 30]:

$$\sigma_{cr} = \frac{4\pi^2 \cdot E \cdot I_x}{L^2 \cdot A}, \quad (1)$$

where σ_{cr} is the critical stress of a column under axial compression, ‘ E ’ is the axial modulus of the material, ‘ A ’ the cross-sectional area of the bar, ‘ I_x ’ is the moment of inertia with respect to x -axis. In the present model, ‘ A ’ and ‘ I_x ’ can be calculated according to the following formula.

$$A = \pi \cdot d \cdot t, \quad (2)$$

$$I_x = \frac{1}{2} \int_0^{2\pi} d\theta \int_{(d-t)/2}^{(d+t)/2} r^3 dr = \frac{A}{8} (d^2 + t^2), \quad (3)$$

where ‘ t ’ is the thickness of the tube, which is 0.2132 nm for SLBP. Hence, equation (1) can be modified as

$$\sigma_{cr} = \frac{\pi^2 \cdot E \cdot (d^2 + t^2)}{2L^2} = \frac{\pi^2}{2} E \cdot \left[\left(\frac{1}{\alpha} \right)^2 + \left(\frac{t}{L} \right)^2 \right]. \quad (4)$$

For the five BPNTs, the elastic moduli are identical. If, for example, the value of α is identical, too, the tube with the lower length will have a higher value of critical stress of buckling. This matches very well with the results given in figure 2(a).

Making use of equation (4), the elastic modulus of a BPNT with its axis normal to the armchair direction can be calculated as 48.255 GPa (NA = 14). This modulus is very close to the results published in [12, 14, 15].

Figure 2(b) shows the potential energy due to deformation. The time at the peak value of deformation potential energy (DPE) is longer than that at the peak value of the stress. With the increase of NA, the difference between them tends to be zero. For example, when NA = 14, the difference is $0.8245 - 0.7830$ (=0.0415 nm), which means 83 loads

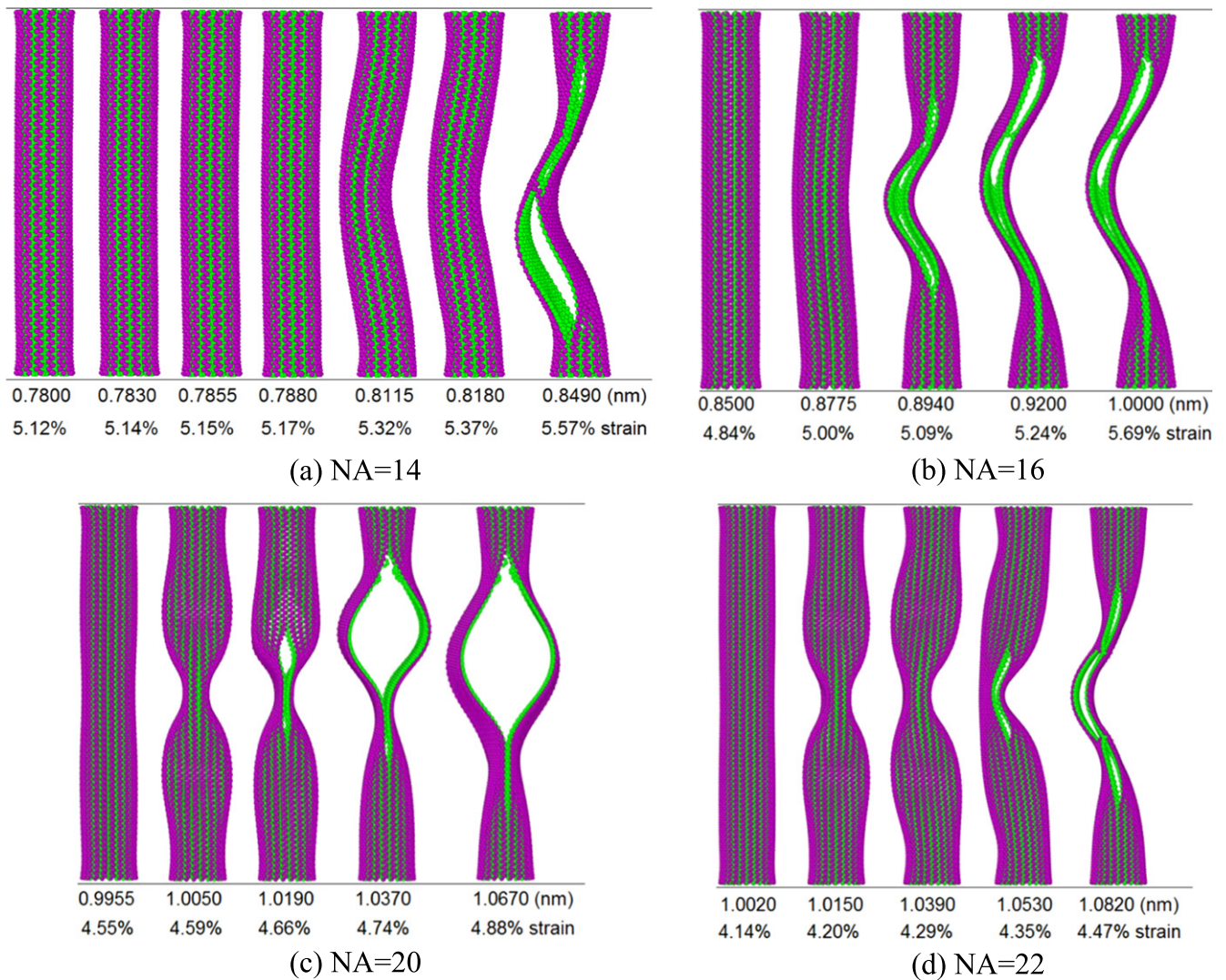


Figure 3. The configurations of the BPNTs during compression. For example, (a) for the tube with $NA = 14$, the compressed length (ΔL) is in $[0.7800, 0.8490]$ nm. Strain is calculated using $\Delta L/L$. The lower end of tube is fixed and the upper end moves down.

steps of difference. When $NA = 22$, the difference is $1.0590 - 1.0560 (=0.0030$ nm), which is only 6 load steps of difference. In each curve of DPE, the value varies in three stages. Firstly, the value increases monotonically with the peak value. The structure deforms linearly in this period. Secondly, the value decreases (but not necessarily monotonically) to the lowest value. This is because the tube is in the buckling state. Finally, as the structure is still in compression, some of the P-P bonds are broken (see figure 3) and the deformation (curvature of tube wall) increases, which leads to the increase of the DPE.

There is a vibration for the transversal deformation of the BPNT with $NA = 14$ during $[0.7800, 0.8490]$ nm of compressed length (see supplementary movie 1, stacks.iop.org/NANO/27/275701/mmedia). The vibration is also reflected in the stress history, as shown by the black data points circled in the figure 2(a). At 0.7830 nm of compressed length, the axial stress of the tube reaches its maximal value of 3.900 GPa. The stress drops to 2.0304 GPa at 0.8115 nm of compressed length. Then the stress increases to a local

maximal value of 2.475 GPa at 0.8180 nm. Soon after that, at 0.8490 ps, fracturing of the tube occurs. As the maximal stress (or critical stress) is approached, the tube can be considered as in a buckling state [29, 31, 32]. But this is only suitable for short tubes. When the length of the BPNT is higher, the tube will be severely broken at the critical stress state. For example, for the BPNT with $NA = 20$, the stress reaches its peak value when the compressed length equals 1.0450 nm. From the third and the fourth configurations of the BPNT with $NA = 20$ in figure 3(c), one can find that the BPNT has been broken severely (supplementary movie 2). Hence, the maximal stress of the tube cannot be considered as the critical stress of the first-ordered buckling.

In the post-buckling state [32–34], the fracture of the tube is due to bond breakage as the curvature of the outer wall of the BPNT is too large [26]. In other words, the BPNT loses stability before the critical state of the strength of the tube. The configurations in figure 3 demonstrate that the critical strain with respect to the strength of a tube decreases with increasing diameter. In addition, the deformation of the tubes

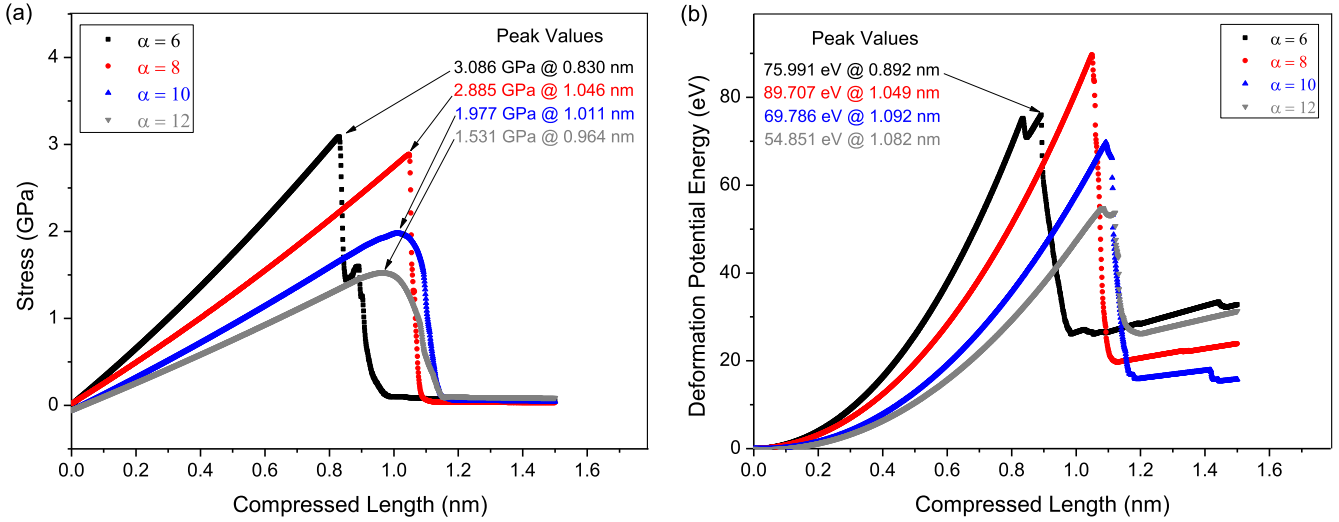


Figure 4. The stress and deformation potential energy of BPNTs (with the same $NA = 20$) under compression. (a) The stress-compressed length curve. (b) The deformation potential energy-compressed length curve. The initial potential energy of the four cases is -2161.28 ($\alpha = 6$), -2864.74 ($\alpha = 8$), -3589.48 ($\alpha = 10$) and -4314.25 eV ($\alpha = 12$), respectively.

before fracture is very small (e.g., 0.8490 nm is only 5.57% of the effective length of tube with $NA = 14$), which indicates that the tubes are in the linear elastic deformation state. Hence, equation (1) is suitable for the current models.

3.2. Length effect on the strength and stability of BPNTs

To demonstrate the influence of the tube length on the strength and stability, in this section, BPNTs with $NA = 20$ ($d = 2.785$ nm) are adopted in the simulation. Four values of tube length are considered: $\alpha = L/d = 6, 8, 10$ and 12 . When $\alpha = 8$, the model is identical to model 4 (with $NA = 20$) in table 1. The major steps in the simulation are similar to those mentioned above. The only difference is that the velocity of loading is set with $s = 0.001$ nm followed with 2 ps of relaxation (i.e., $t_R = 2$ ps).

It can be seen from figure 4(a) that the critical stress (the peak value of stress) is higher for a shorter tube under compression. This agrees well with equation (4). However, the time when the stress approaches the peak value does not obey the rule well. Before buckling, the tube is in a linear elastic state. Hence, the critical strain can be expressed as

$$\varepsilon_{cr} = \frac{\sigma_{cr}}{E} = \frac{\pi^2 \cdot (d^2 + t^2)}{2L^2}. \quad (5)$$

From the definition of strain of a column, the critical strain can be expressed as

$$\varepsilon_{cr} = \frac{\Delta L_{cr}}{L}, \quad (6)$$

where ΔL_{cr} is the critical value of compressed length of a BPNT. Hence, we have

$$\Delta L_{cr} = \frac{\pi^2 \cdot (d^2 + t^2)}{2L}. \quad (7)$$

The results shown in figure 4 are obtained by investigating BPNTs with the same cross section (i.e., the same values of d and t) but different lengths under the same loading condition. Hence, equation (7) indicates that the critical value of the compressed length of a BPNT is inversely proportional to its length. But this is not satisfied for $\alpha = 6$ (the shortest tube). When $\alpha = 6$, the critical compressed length is the smallest rather than the greatest among the four cases, because the critical stress appears earlier than the critical strain for the shortest tube.

Figure 4(b) shows the DPE of tubes with different lengths, in which the peak value of the DPE of the tube with $\alpha = 6$ is lower than that of the tube with $\alpha = 8$. The reason is that the tube with $\alpha = 6$ is shorter and the compressed length is also lower than that of the tube with $\alpha = 8$. The DPE of the tube with $\alpha = 8$ is also higher than those of the tubes with $\alpha = 10$ and 12 . The reason is that the tube of $\alpha = 8$ has a higher value of critical stress and larger compressed length.

Figure 5 gives five representative configurations of the tube under compression. Comparing it with figure 4(a), the peak value of stress appears before fracture starts. Commonly, the tubes were in the post-buckling state when their stress approaches maximum. One can also find that the critical strain with respect to the strength decreases with an increase in the length. For example, the critical strain is between (4.99% and 5.22%) when $L = 6d$ ($\alpha = 6$, figure 5(a)) (supplementary movie 3). When $L = 8d$ ($\alpha = 8$, figure 5(b)), the critical strain is between (4.58% and 4.83%). If the length of tube is 12 times the diameter, the critical strain is lower than 3.23% (the third configuration in figure 5(d)).

3.3. Effect of load speed on the strength and stability of BPNTs

In this section, the effect of loading speed on the strength and stability of BPNT is discussed. The BPNT with $NA = 20$ ($d = 2.785$ nm) and $L = 20.166$ nm is adopted in the

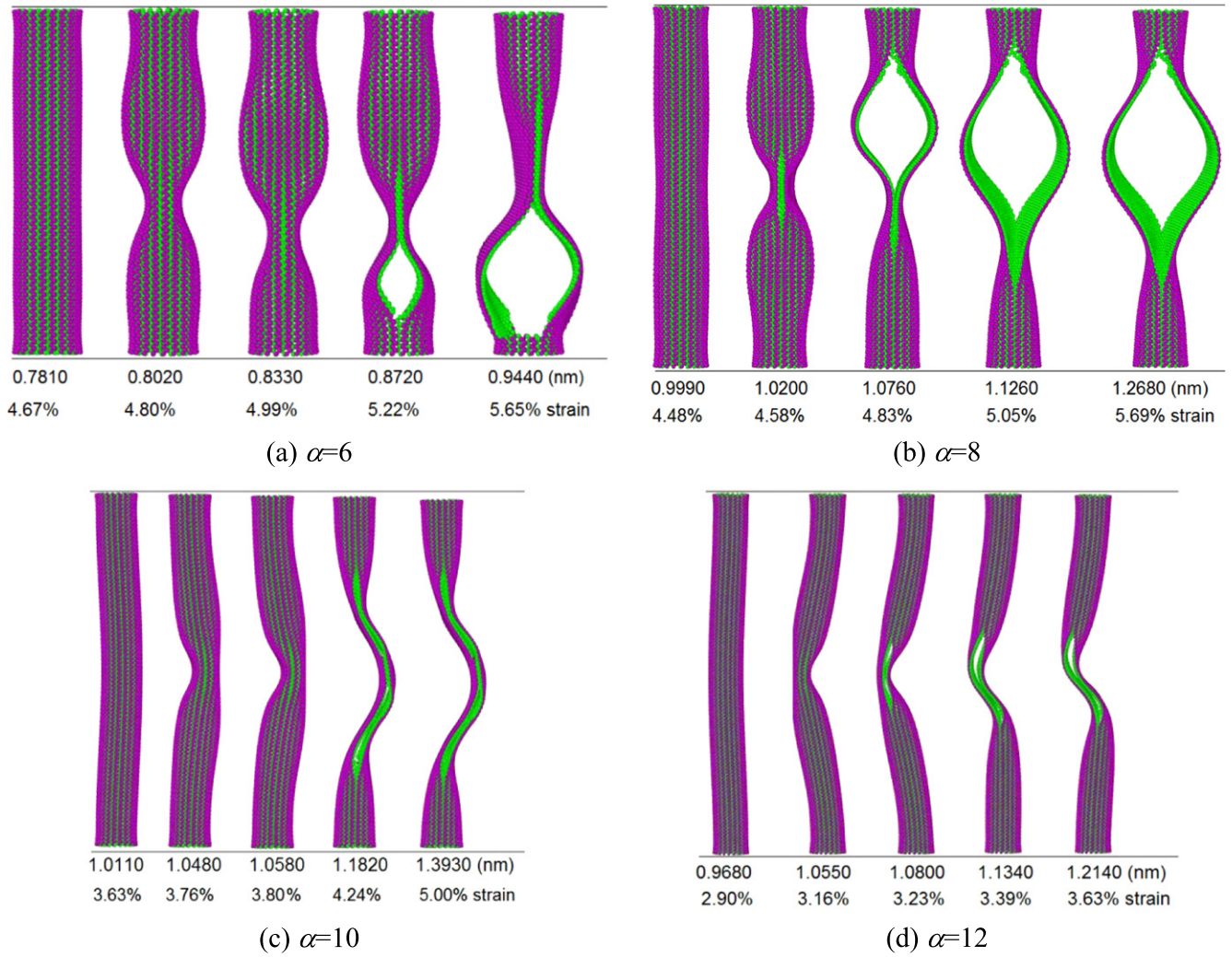


Figure 5. Representative configurations of BPNTs with different lengths during compression ($\alpha = L/d$).

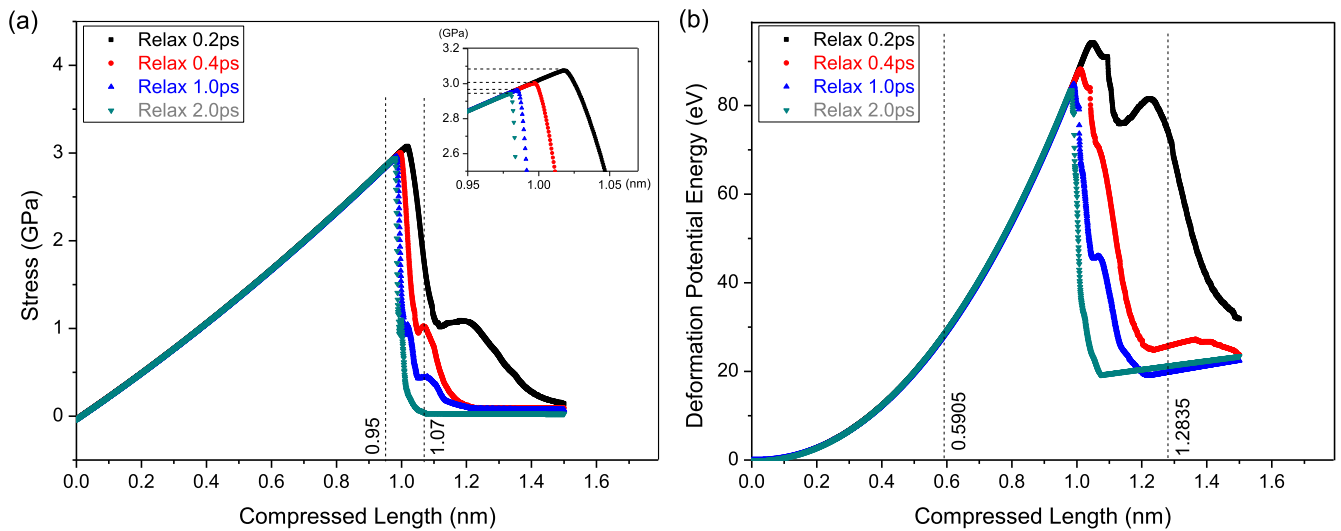


Figure 6. The stress and deformation potential energy of the same BPNT ($NA = 20, L = 20.166 \text{ nm}$) under compression with different load speeds, i.e., in each load step the relaxation time is 0.2, 0.4, 1.0 and 2.0 ps. (a) The stress-compressed length curve. The peak values are 3.075 GPa at 1.0175 nm ($t_R = 0.2 \text{ ps}$), 3.002 GPa at 0.9970 nm ($t_R = 0.4 \text{ ps}$), 2.960 GPa at 0.9850 nm ($t_R = 1.0 \text{ ps}$) and 2.9433 GPa at 0.9800 nm ($t_R = 2.0 \text{ ps}$), respectively. (b) The deformation potential energy-compressed length curve. The initial potential energy of the four cases is -587.59 eV .

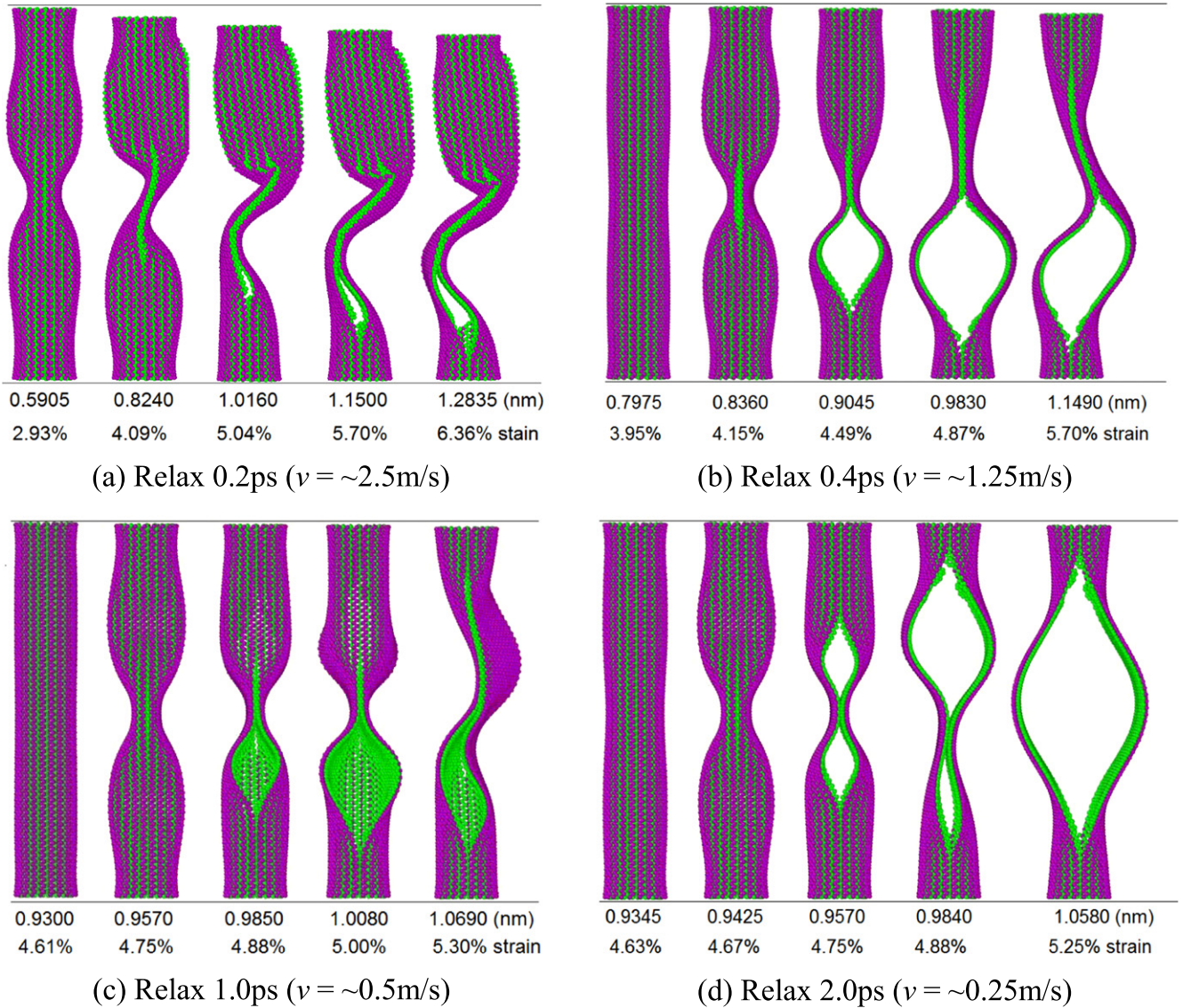


Figure 7. Representative snapshots of the BPNT ($NA = 20$, $L = 20.166$ nm) during compression with different loading speeds.

simulation. All major steps in our simulation are identical to those described in section 3.1 except for the loading step. Four types of loading speed (or relaxation schemes) are considered, i.e., $s = 0.0005$ nm followed with $t_R = 0.2, 0.4, 1.0$ and 2.0 ps of relaxation in each load step, or respectively, the loading velocities are $\sim 2.5, 1.25, 0.5$ and 0.25 m s^{-1} .

Figure 6(a) indicates that the peak value of the critical stress of the BPNT is higher at higher loading speed. The stress gains its highest value when there is only 0.2 ps of relaxation in each load step. But the differences among the peak values are not obvious. Figure 6(b) shows that the tube under the first relaxation scheme also has the highest potential energy. The reason is that the tube has a higher value of compressed length before buckling or fracture.

Figure 7 gives five snapshots of the tube under load with different lengths of relaxation in each step for each case. Clearly, the tube is in the buckling state when the compressed length is 0.5905 nm for $t_R = 0.2$ ps. When the compressed length reaches 0.8240 nm, the tube is fractured. After that, the

tube collapses. In this case, the configuration is with respect to 1.0160 nm of compressed length or 5.04% of engineering strain (figure 7(a)) (supplementary movie 4). For the four cases, the strain of the BPNT, which is still in the post-buckling state but not damaged, is higher at lower loading speed, e.g., 2.93% ($t_R = 0.2$ ps) $<$ 3.95% ($t_R = 0.4$ ps) $<$ 4.61% ($t_R = 1.0$ ps) $<$ 4.63% ($t_R = 2.0$ ps).

3.4. Effect of temperature on the strength and stability of BPNTs

In the discussion above, the temperature is set to be 0.1 K. This means that the results obtained have nothing to do with the thermal vibration of atoms on tubes. In reality, devices commonly run at different temperatures. Hence, the temperature is also an important factor that can affect the strength and stability of BPNTs. The major steps in our simulation are largely similar to those described above. The only difference

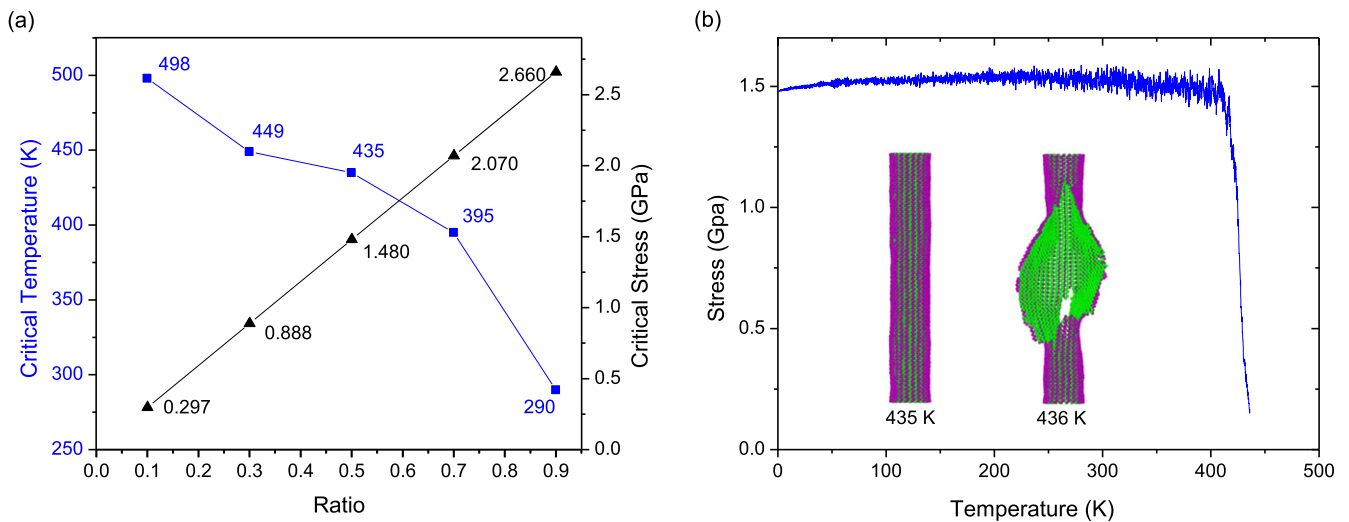


Figure 8. (a) The critical temperature and stress of the BPNT ($NA = 20$, $L = 20.166$ nm) with specified compressed length. The ratio is the specified compressed length over 0.9800 nm. (b) The stress history of the BPNT with 0.5 times 0.9800 nm compressed length with increasing temperature.

is that the environmental temperature increases from 0.1 K at a speed of 1 K ps^{-1} .

The BPNT used in this section is the same as that in section 3.3, with $NA = 20$, $L = 20.166$ nm. From the discussion above, we know that the tube buckles when the compressed length approaches 0.9800 nm (with a relaxation for 2 ps in each load step). As shown in our previous study [26], stronger thermal vibration of the atoms on the BPNT leads to easier failure of structure. Hence, we believe that the compressed length will be shorter at higher temperature for the same BPNT. In the present simulation, we chose the maximal compressed lengths of the BPNT to be 0.1 , 0.3 , 0.5 , 0.7 and 0.9 times the 0.9800 nm. In each loading step, $s = 0.0005$ nm followed with 2.0 ps of relaxation. When the compressed length reaches the specified value, the environmental temperature starts to increase until the tube is in the buckling state or fractured.

From figure 8(a), we find that the BPNT with a shorter compressed length can bear higher temperatures before failure of the nanostructure. The temperature at which the tube fails is called the critical temperature of the tube with specified compressed length. For instance, the critical temperature reaches 498 K when the tube is subjected to 0.1 times the 0.9800 nm of compressed length. When the tube has a compressed length of 0.9 times 0.9800 nm, the critical temperature approaches 290 K. It means that the present BPNT (with $NA = 20$, $L = 20.166$ nm) has high resistance to environmental temperature. The critical stress of the tube however is still approximately proportional to the compressed length.

In figure 8(b), the stress of the tube is stable during the process of increasing the temperature before reaching 400 K. When the temperature is higher than 420 K, the stress drops rapidly. This is because buckling happens. In particular, at 436 K, the tube is broken (see the inset figures and supplementary movie 5). It demonstrates that the critical temperature given in figure 8(a) is actually higher than the temperature at which the tube starts buckling. Hence, the critical temperature

of 436 K, is the upper boundary of the temperature for tube to be fractured. Considering this phenomenon, a nanodevice with such a BPNT as a component should operate at a temperature lower than the critical temperature.

If a continuous loading approach (fixed velocity of top end of tube) is used, the results will be different. For example, for our present scheme, the system has a period to adjust the states of atoms (positions and velocities), and the loading area (top end) has no continuous velocity. In a canonical NVT ensemble, the adjustment of velocities of atoms with respect to the difference between the ‘present temperature’ and the constraint value (e.g., 300 K) depends very slightly on the loading step. If using a continuous loading approach, the velocities of the atoms near the loading area have some influence on the adjustment. Of course, if the length of relaxation time after loading is very close to the time step, the difference between the two loading schemes can be neglected.

4. Conclusion

Considering the importance of the mechanical properties of a BPNT on the design of a nanodevice with a BPNT as a component, the strength and stability of a BPNT under compression were numerically investigated. From the results, some conclusions are made as follows,

1. The BPNT starts buckling, which is followed by fracturing. Before fracturing, the structure has very small axial strain ($\sim 5\%$), hence, the buckling state of a BPNT can be controlled with Euler’s buckling formula.
2. For a tube with the same ratio of length over diameter, the critical strain with respect to the strength of a tube decreases with increasing diameter.
3. For a tube with the same cross section, the critical stress (the peak value of stress) is higher for a shorter tube

under compression. The critical strain with respect to the strength decreases with increasing length.

4. For the same BPNT under load with different speeds, the strain of the BPNT, which is still at the post-buckling state but not damaged, is higher at lower loading speed.
5. The same BPNT can withstand a higher temperature when under lower compressed length. Hence, a nanodevice with a BPNT as a component should work at a temperature lower than the critical temperature with respect to strength.

Acknowledgment

Financial support from the National Natural Science-Foundation of China (Grant No.11372100) is acknowledged.

References

- [1] Li L, Yu Y, Ye G J, Ge Q, Ou X, Wu H, Feng D, Chen X H and Zhang Y 2014 Black phosphorus field-effect transistors *Nat. Nanotechnol.* **9** 372–7
- [2] Liu H, Neal A T, Zhu Z, Luo Z, Xu X, Tománek D and Ye P D 2014 Phosphorene: an unexplored 2D semiconductor with a high hole mobility *ACS Nano* **8** 4033–41
- [3] Rodin A, Carvalho A and Neto A C 2014 Strain-induced gap modification in black phosphorus *Phys. Rev. Lett.* **112** 176801
- [4] Li W, Yang Y, Zhang G and Zhang Y-W 2015 Ultrafast and directional diffusion of lithium in phosphorene for high-performance lithium-ion battery *Nano Lett.* **15** 1691–7
- [5] Novoselov K S, Geim A K, Morozov S, Jiang D, Zhang Y, Dubonos S A, Grigorieva I and Firsov A 2004 Electric field effect in atomically thin carbon films *Science* **306** 666–9
- [6] Lee C, Wei X, Kysar J W and Hone J 2008 Measurement of the elastic properties and intrinsic strength of monolayer graphene *Science* **321** 385–8
- [7] Golberg D, Bando Y, Huang Y, Terao T, Mitome M, Tang C and Zhi C 2010 Boron nitride nanotubes and nanosheets *ACS Nano* **4** 2979–93
- [8] Zhi C, Bando Y, Tang C, Kuwahara H and Golberg D 2009 Large-scale fabrication of boron nitride nanosheets and their utilization in polymeric composites with improved thermal and mechanical properties *Adv. Mater.* **21** 2889–93
- [9] Liu H, Neal A T and Ye P D 2012 Channel length scaling of MoS₂ MOSFETs *ACS Nano* **6** 8563–9
- [10] Radisavljevic B, Radenovic A, Brivio J, Giacometti V and Kis A 2011 Single-layer MoS₂ transistors *Nat. Nanotechnol.* **6** 147–50
- [11] Appalakondaiah S, Vaitheeswaran G, Lebegue S, Christensen N E and Svane A 2012 Effect of van der Waals interactions on the structural and elastic properties of black phosphorus *Phys. Rev. B* **86** 035105
- [12] Jiang J W and Park H S 2014 Mechanical properties of single-layer black phosphorus *J. Phys. D: Appl. Phys.* **47** 385304
- [13] Jiang J W and Park H S 2014 Negative Poisson's ratio in single-layer black phosphorus *Nat. Commun.* **5** 4727
- [14] Wei Q and Peng X 2014 Superior mechanical flexibility of phosphorene and few-layer black phosphorus *Appl. Phys. Lett.* **104** 251915
- [15] Wang Z, Jia H, Zheng X, Yang R, Wang Z, Ye G, Chen X, Shan J and Feng P X-L 2015 Black phosphorus nanoelectromechanical resonators vibrating at very high frequencies *Nanoscale* **7** 877–84
- [16] Sorkin V and Zhang Y 2015 The structure and elastic properties of phosphorene edges *Nanotechnology* **26** 235707
- [17] Hu T, Han Y and Dong J 2014 Mechanical and electronic properties of monolayer and bilayer phosphorene under uniaxial and isotropic strains *Nanotechnology* **25** 455703
- [18] Yang Z, Zhao J and Wei N 2015 Temperature-dependent mechanical properties of monolayer black phosphorus by molecular dynamics simulations *Appl. Phys. Lett.* **107** 023107
- [19] Sha Z D, Pei Q X, Ding Z, Jiang J W and Zhang Y W 2015 Mechanical properties and fracture behavior of single-layer phosphorene at finite temperatures *J. Phys. D: Appl. Phys.* **48** 395303
- [20] Qiu W, Kang Y L, Lei Z K, Qin Q H and Li Q 2009 A new theoretical model of a carbon nanotube strain sensor *Chin. Phys. Lett.* **26** 080701
- [21] Cai K, Yin H, Qin Q H and Li Y 2014 Self-excited oscillation of rotating double-walled carbon nanotubes *Nano Lett.* **14** 2558–62
- [22] Cai K, Li Y, Qin Q H and Yin H 2014 Gradientless temperature-driven rotating motor from a double-walled carbon nanotube *Nanotechnology* **25** 505701
- [23] Qin Z, Qin Q H and Feng X Q 2008 Mechanical property of carbon nanotubes with intramolecular junctions: molecular dynamics simulations *Phys. Lett. A* **372** 6661–6
- [24] Qiu W, Kang Y L, Lei Z K, Qin Q H, Li Q and Wang Q 2010 Experimental study of the Raman strain rosette based on the carbon nanotube strain sensor *J. Raman Spectrosc.* **41** 1216–20
- [25] Guo H, Lu N, Dai J, Wu X and Zeng X C 2014 Phosphorene nanoribbons, phosphorus nanotubes, and van der Waals multilayers *J. Phys. Chem. C* **118** 14051–9
- [26] Cai K, Wan J, Wei N, Cai H F and Qin Q H 2015 Temperature effect on failure of a free nanotube from single-layer black phosphorus *Nanotechnology* **27** 235703
- [27] Plimpton S 1995 Fast parallel algorithms for short-range molecular dynamics *J. Comput. Phys.* **117** 1–19
- [28] Jiang J W, Rabczuk T and Park H S 2015 A Stillinger–Weber potential for single-layered black phosphorus, and the importance of cross-pucker interactions for a negative Poisson's ratio and edge stress-induced bending *Nanoscale* **7** 6059–68
- [29] Koiter W T 1945 On the stability of elastic equilibrium *PhD Thesis* Technological University of Delft
- [30] Jones R M 2006 *Buckling of Bars, Plates and Shells* (Blacksburg: Bull Ridge Corporation)
- [31] Cai K, Gao D Y and Qin Q H 2014 Post-buckling solutions of hyper-elastic beam by canonical dual finite element method *Math. Mech. Solids* **19** 659–71
- [32] Cai K, Gao D Y and Qin Q H 2014 Postbuckling analysis of a nonlinear beam with axial functionally graded material *J. Eng. Math.* **88** 121–36
- [33] Qin Q H 1997 Postbuckling analysis of thin plates on an elastic foundation by HT FE approach *Appl. Math. Modell.* **21** 547–56
- [34] Qin Q H and Huang Y 1990 BEM of postbuckling analysis of thin plates *Appl. Math. Modell.* **14** 544–8